A RC fibre beam element for full modelling of the bending-shear response by dual section approach

P. Tortolini, E. Spacone, M. Petrangeli

Department of Engineering, University "G. D'Annunzio"of Chieti Pescara, Italy

SSCS 2012 Numerical Modeling Strategies for Sustainable Concrete Structures

Aix-en-Provence, France
May 29-June 1, 2012

1.Introduction

Although a wide number of non-linear reinforced concrete beam-column models are available, only a few can properly account for the shear response and its interaction with bending and axial forces. The existing models (an exhaustive state of the art can be found in [1]) can be grouped in the following three categories:

- strut and tie models [1] [2] [3];
- microplane fibre models [4] [5];
- MCTF or smeared crack fibre models [6] [7] [8].

The model presented in this paper belongs to the second group as it stem from the research work carried out on fibre models by Italian researchers in the 90s. Its force-based algorithm iterative solutions were developed by Spacone et al. [9] and Petrangeli and Ciampi [10]. The element presented here is an evolution of previous models and the corresponding computer code developed by Petrangeli [4-5]. The shear section modelling is enhanced by enforcing equilibrium between two adjacent sections (rather than applying a kinematic constraint for the shear strain distribution over the section). This so-called Dual Section approach introduces an additional iteration loop in the element state determination.

2. The finite element

The element is characterised by a threefold nested structure, namely: Element - Section - Fibre. At the fibre level, material (concrete and steel) constitutive laws are applied. At the section level, integration of the fibre response is carried out in order to obtain the generalised forces (bending, M, axial N, and shear V). Nodal forces are finally found using the equilibrium-based iterative approach [9][10].

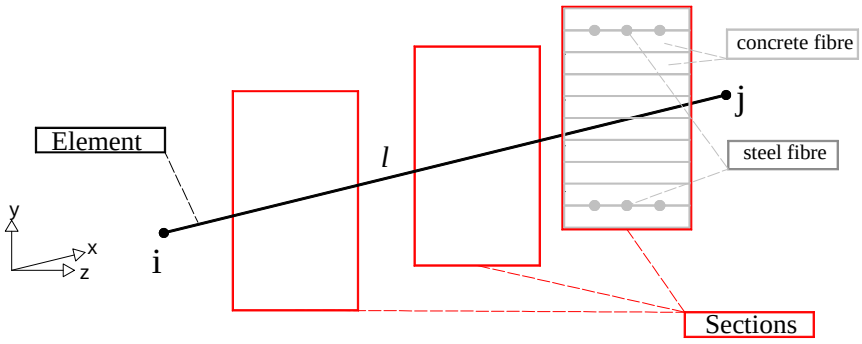

Figure 1: 2D fibre element definition.

2.1. Element state determination

The element deformations Q for a 2D beam without rigid body modes are the following (see figure 2).

$$Q = \left[\varepsilon, r_i, r_j\right]^T \tag{1}$$

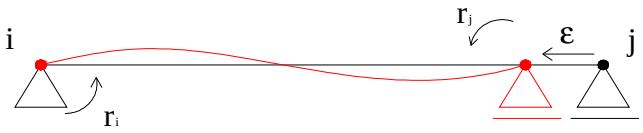

Figure 2: Beam static configuration and kinematic mechanisms (without rigid body modes).

The corresponding nodal forces P are:

$$P = \left[N, M_i, M_j\right]^T \tag{2}$$

The section generalised deformations q (axial, curvature and shear deformations) are written as follows:

$$q(x) = \left[\varepsilon, \varphi(x), \gamma(x)\right]^T \tag{3}$$

The corresponding section generalised stresses p are:

$$p(x) = \left[N, M(x), V(x)\right]^T \tag{4}$$

Equilibrium between section generalises force and element nodal forces is imposed as follows:

$$p(x) = b(x) \cdot P \tag{5}$$

where $b(x)$ is a matrix containing stress shape functions along the element, also known as equilibrium integrals, obtained exclusively from beam equilibrium conditions.

The relationship between nodal and generalised section deformations are found by applying the virtual work principle as shown below:

$$Q = \int_l b(x)^T \, q(x) dx \tag{6}$$

The section generalised stresses are found integrating the fibre response. Fibre stress-strain relations are explicit algebraic expressions and so are the section generalised stresses as a function of the section deformations, except for the nested loop required to define shear deformations imposing equilibrium (dual section approach) as specified hereafter:

$$p(x) = p\big(q(x)\big) \tag{7}$$

For any given increment of element deformations ΔQ, the corresponding increment in the section field is found as thea sum of a particular solution $\Delta q_0(x)$ plus a series of homogeneous function $rq_i(x)$:

$$\Delta q_i(x) = \Delta q_0(x) + \sum_i rq_i(x) \tag{8}$$

with

$$\Delta Q = \int_l b(x)^T \, \Delta q_0(x) dx \tag{9}$$

The homogeneous function $rq_i(x)$ are found imposing equilibrium between the element nodal forces and the internal section force field:

$$rp_i(x) = b(x)\Delta P_i - \Delta p_{i-1}(x) \tag{10}$$

$$rq_i(x) = f(x) \; rp_i(x) \tag{11}$$

where *f(x)* is the section flexibility matrix.

Imposing the homogeneity condition of the above correction terms:

$$\overline{0} = \int_l b(x)^T \, rq_i(x) dx$$

implies that:

$$\Delta P_i = F^{-1} \int_l b(x)^T \, f(x) \; \Delta p_{i-1}(x) dx \tag{12}$$

where F is the element stiffness matrix:

$$F = \int_l b(x)^T \, f(x) \; b(x) dx \tag{13}$$

In eqn. (12), it is shown that element forces at the *i-th* iteration are solely dependent upon the previous iteration. The iterative correction process ends (that is, convergence is reached), when the average value of the difference along the element given by eqn. (10) is acceptable:

$$\int_l rp_i(x)^T \, f(x) \; rp_i(x) dx \le E_{unb} \tag{14}$$

A visual description of eqn. (10) is presented in figure 3.

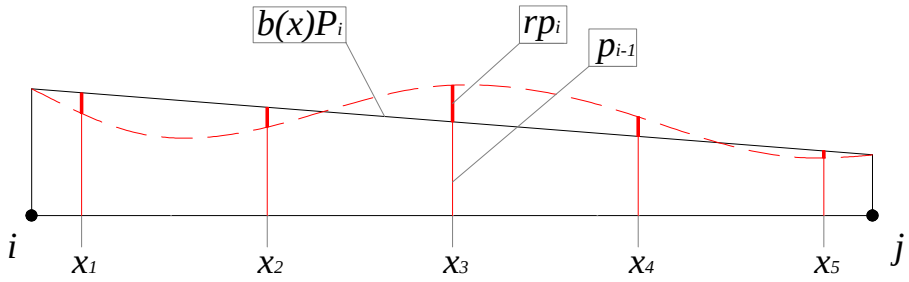

Figure 3: Element state determination

2.2. Section state determination

At the section level generalised section stresses, *p(x)*, are obtained by integration of the fibre response (stresses). Steel and concrete fibres are identified and characterised by their relative surface area and position at the monitored section.

In the presence of both constant section geometry and reinforcement distribution along the element length, these variables become section *(x)*- independent:

$$A^s_{xx,j} \quad , \quad y^s_j \qquad j = 1 \ldots n_{fs}$$

$$A^c_{xx,k} \quad , \quad y^c_k \qquad k = 1 \ldots n_{fc}$$

where the $^{s/c}$ superscript and the $_{k/j}$ subscripts identify fibre types (*s=steel*, *c=concrete*) and individual fibre, respectively.

In order to model both normal and shear stresses, the concrete constitutive model is two dimensional and therefore concrete transverse surface area *y* need to be specified

$$A^c_{yy,k} \qquad k = 1 \ldots n_{fc}$$

as well as the corresponding amount of transverse reinforcement (hoops) ratio in the same direction (figure 4):

$$\rho_{yy,k} = A^s_{yy,k} / A^c_{yy,k} \qquad k = 1...n_{fc}$$

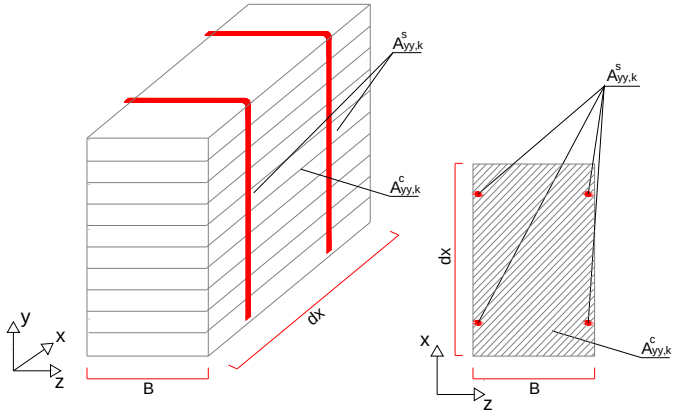

Figure 4: Transversal cross section concrete definition.

The longitudinal steel fibres have a uniaxial behaviour only. The rather sophisticated cyclic stress-strain behaviour is based on an existing formulation [11]:

$$\sigma^s_{xx} = f(\varepsilon^s_{xx}) \tag{15}$$

The concrete constitutive behaviour is based on the microplane model:

$$\sigma^c = D(\varepsilon^c) \tag{16}$$

where σ^c and ε^c are the 2D concrete stress and strain tensors:

$$\sigma^c = [\sigma^c_{xx}; \sigma^c_{yy}; \tau^c_{xy}]$$
$$\varepsilon^c = [\varepsilon^c_{xx}; \varepsilon^c_{yy}; \varepsilon^c_{xy}]$$

The fibre longitudinal deformations are obtained from the section axial deformation and curvature assuming plane sections and perfect bond conditions:

$$\varepsilon^s_{xx,j} = \varepsilon - \varphi(x) \cdot y^s_j \quad , \quad j=1...n_{fs} \tag{17}$$

$$\varepsilon^c_{xx,k} = \varepsilon - \varphi(x) \cdot y^c_k \quad , \quad k=1...n_{fc} \tag{18}$$

The concrete lateral deformation is obtained imposing equilibrium between concrete fibres and steel transverse reinforcement. The latter uses a simplified elasto-plastic stress-strain relationship *f(ε)*:

$$\sigma^c_{yy,k} + \rho_{yy,k} f(\varepsilon_{yy,k}) = 0 \tag{19}$$

The solution to eqn. (19) requires an iterative procedure (fibre iterations). Starting from an initial tentative solution ($\varepsilon^{c,0}_{yy,k}$), calculated assuming linear elastic isotropic behaviour of the concrete fibres, correction terms are added until equilibrium is reached (i.e. eqn. (19) is satisfied).

$$\varepsilon^c_{yy,k} = \varepsilon^{c,0}_{yy,k} + \varepsilon^{c,1}_{yy,k} + ... + \varepsilon^{c,i}_{yy,k} = 0 \tag{20}$$

Finally, concrete fibre shear deformation is obtained using the *Dual Section (DS)* approach as initially proposed by Vecchio and Collins [6]. This approach is based on the beam differential equilibrium equation:

$$\frac{dM}{dx} = V \tag{21}$$

When this equation is applied at the section level we can find the concrete fibre shear forces as a function of the variation in longitudinal (axial) forces of the same fibres between two adjacent

sections.

$$F_{xy,k} = \left(F^{c}_{xx,1-k}(x_{n+1}) + F^{s}_{xx,1-k}(x_{n+1})\right) - \left(F^{c}_{xx,1-k}(x_{n}) + F^{s}_{xx,1-k}(x_{n})\right) \tag{22}$$

Re-arranging eqn. (22) in stress terms, the shear stress in the *k-th* fibre is expressed as:

$$\tau^{c}_{xy,k}\,|_{DS} = \frac{\sum_{1}^{k}\sigma^{c}_{xx,k}(x_{n+1})A^{c}_{xx,k} - \sum_{1}^{k}\sigma^{s}_{xx,k}(x_{n+1})A^{s}_{xx,k}}{B\cdot(x_{n+1}-x_{n})} - \frac{\sum_{1}^{k}\sigma^{c}_{xx,k}(x_{n})A^{c}_{xx,k} - \sum_{1}^{k}\sigma^{s}_{xx,k}(x_{n})A^{s}_{xx,k}}{B\cdot(x_{n+1}-x_{n})} \tag{23}$$

where *B* is the section width (a constant rectangular section along the beam length is assumed here).

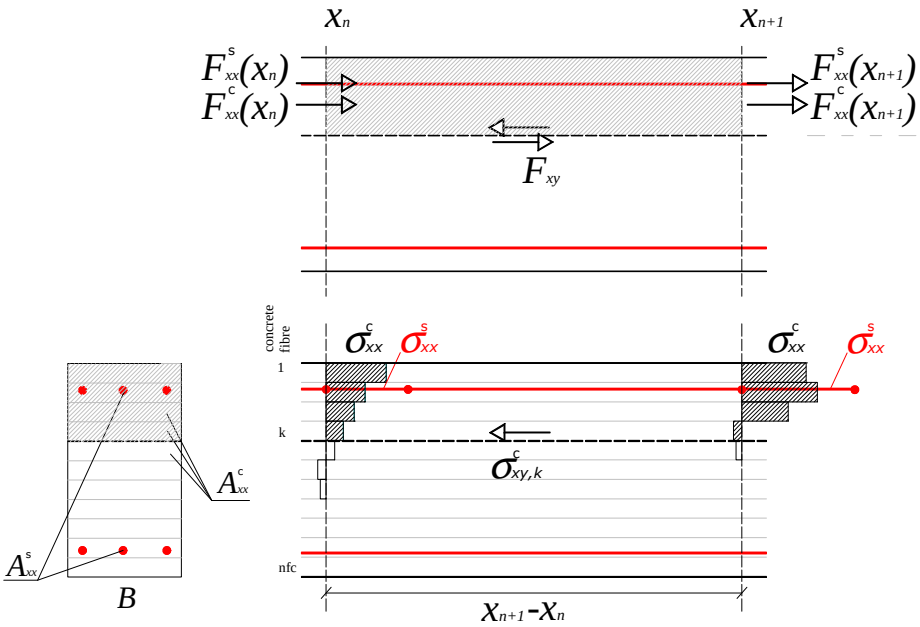

Figure 5: Dual section approach.

The fibre shear stresses, found at each load increment starting from a fibre shear strain increment calculated assuming linear elastic isotropic concrete behaviour, do not generally satisfy equilibrium as stated in eqn. (23). A corrective procedure is implemented, similarly to what is done for the fibre transverse equilibrium.

Unlike transverse equilibrium, the shear strain corrective terms needed to satisfy equilibrium must be homogeneous, that is their integral over the section must be null. The shear strain corrective terms are calculated using the shear stress residuals ($r\tau^{c}_{xy,k}$) and the concrete elastic shear modulus (G) is used to get the shear deformation residual:

$$\tau^{c}_{xy,k} - \tau^{c}_{xy,k}\,|_{DS} = r\tau^{c}_{xy,k} \tag{24}$$

$$r\varepsilon^{c}_{xy,k} = \frac{r\tau^{c}_{xy,k}}{G} \tag{25}$$

The fibre shear deformation corrections calculated with eqn.(25) are not homogeneous though. The section shear increment associated to these deformations is:

$$R_{\gamma}(x) = \frac{\sum_{k=1}^{nfc} r\varepsilon^{c}_{xy,k}A^{c}_{xx,k}}{\sum_{k=1}^{nfc} A^{c}_{xx,k}} \tag{26}$$

The fibre homogeneous shear strain corrective term is finally given by the value found from equilibrium, that is eqn.(25) minus the expressione calculated with eqn. (26). Since eqn. (26) gives the

section integral, a shape function must be used to calculate each fibre value. This shape function can be the same shape function used to calculate the particular solution (initial shear strain increment) as discussed hereafter. Finally, the iterative solution of shear strain distribution for each fibre can be written as:

$$\varepsilon^{c}_{xy,k} = g(y_k)\gamma(x) + \left(r\varepsilon^{c,1}_{xy,k} - g(y_k)R^{1}_{\gamma}(x)\right) + \ldots + \left(r\varepsilon^{c,i}_{xy,k} - g(y_k)R^{i}_{\gamma}(x)\right) \tag{27}$$

where the first term is the particular solution, calculated using a given shape function *g(y)*. Again, the standard parabolic distribution is fine but a normalized shape function of the actual section shear field at any given step is also very effective. This procedure ends when a satisfactory tolerance threshold is satisfied over the entire section:

$$\sum_{k=1}^{nfc}\left(\tau^{c,i}_{xy,k} - \tau^{c,i}_{xy,k}\mid_{DS}\right)A^{c}_{xx,k} = R_{\tau} \le R_{unb} \tag{27}$$

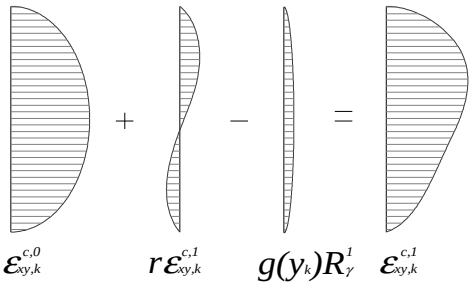

Figure 6: Dual section iterative procedure.

The above describe procedure cannot be carried out fibre by fibre – following the correction of the lateral strain, eqn. (20) – but all residual fibre shear strains over the sections need to be calculated in order to carry out the homogeneous corrective procedure, eqn. (24) to eqn. (27). The procedure can therefore only be carried out at a section level (section iterations), introducing an embedded cycle nested between the element and the fibre iterations.

Finally, once the fibre deformation vectors are found, the stress vectors are computed from the concrete and steel constitutive laws. The fibre stresses are then integrated over the section to compute the generalized section forces to be used in the element equilibrium iterations.

$$N(x) = \sum_{k=1}^{nfc}\sigma^{c}_{xx,k}(x)A^{c}_{xx,k} + \sum_{j=1}^{nfs}\sigma^{s}_{xx,j}(x)A^{s}_{xx,j} \tag{28}$$

$$M(x) = \sum_{k=1}^{nfc}\sigma^{c}_{xx,k}(x)A^{c}_{xx,k}y^{c}_{k} + \sum_{j=1}^{nfs}\sigma^{s}_{xx,j}(x)A^{s}_{xx,j}y^{s}_{j} \tag{29}$$

$$V(x) = \sum_{k=1}^{nfc}\tau^{c}_{xy,k}(x)A^{c}_{xx,k} \tag{30}$$

2.3. Concrete constitutive law

The two-dimensional constitutive law used for the concrete fibres is based on a modified Microplane model [4] [5] [12]. A brief summary of the main model features is presented here.

The constitutive model is developed from classical *microplane* theory [13], where the material behaviour (2D or 3D) is described by a number of surfaces (microplanes) where explicit stress-strain relationships are defined. The global (macroscopic) behaviour is obtained by considering individual microplane contributions. Traditionally, such models are based on kinematic constraints needed to obtain microplane deformations ($e_{k,i}$) from the macroscopic deformation vector (ε) via geometric relationships. The $A_{k,i}$ operator containing the microplane direction cosines is applied to the macroscopic vector to compute the two (i) deformation components (normal and shear components in 2D case) of the *k-th* microplane.

$$e_{k,i} = A_{k,i}^{T} \varepsilon^{c} \tag{31}$$

Making use of the virtual work principle whereby work at a microscopic level is equated to that at the macroscopic level, a correspondence between microplane and macroscopic stresses (on the unit radius circle C) is found:

$$\int_{0}^{2\pi} (ds \cdot de) d\vartheta = 2\pi (d\sigma \cdot d\varepsilon) \tag{32}$$

where terms on the LHS and RHS are referred to as the microscale and macroscale terms, respectively.

The kinematic constraint (31) used in the classical Microplane approach suffers from various drawbacks, especially when it comes to modelling large tensile deformations (cracking). Typically, concrete cracking is modelled using a static approach as in most smeared crack approaches. A proper static constraint at the constitutive level would be very cumbersome and time demanding for the beam model under consideration. A modified Microplane approach was therefore developed by the authors based on strain partitioning.

Due to concrete heterogeneity (cement paste and aggregates), strains can be split into a strong and a weak component. The strong component accounts for the aggregate response, the weak component accounts for the mortar and the interface contribution.

$$\varepsilon^{c} = \varepsilon_{strong}^{c} + \varepsilon_{weak}^{c} \tag{33}$$

The above weak and strong splitting is carried out in the principal tensile directions using explicit algebraic expressions. Unlike smeared crack approaches, where the model response is given by the strong component (linear elastic) once it has been depurated of the weak one (crack) along the principal tensile direction, in the proposed approach, the weak component goes into the microplane model. In the proposed model the weak component is therefore a full 2D strain tensor that is obtained from the total one subtracting the strong component. This latter is found as a function of the strain invariants (volumetric, ε_V, and deviatoric, ε_D), as well as the material deformation properties (peak tensile ε_{ct} and compression ε_{cc} strain).

$$\varepsilon_{strong}^{c} = \Psi_{split}(\varepsilon_V; \varepsilon_D; \varepsilon_{ct}; \varepsilon_{cc}) \cdot \varepsilon^{c} \tag{34}$$

From the above expressions, a comprehensive and realistic representation of concrete behaviour is given under complex loading scenarios [12] [14] by solely considering the microplane orthogonal (normal) component defined by a very simple stress-strain law based on exponential formulations [15]. This microplane stress-strain law has full cyclic capabilities and so does the resulting constitutive 2D behaviour.

3. Numerical analysis results

In order to validate the *Dual Section* shear fibre beam model presented above, a number of experimental tests found in the published literature were numerically simulated. In the following, some of the most significant ones are presented, with the full set available in [14].

The testing campaign carried out at the University of California, Diego on a series of reinforced concrete columns is extensively described and discussed in [16]. Specimens R-1 and R-5 shared the same section dimensions (16” x 24” or 410mm x 610mm) and steel reinforcement along the height, comprising 22 size 6 (=19.05mm) bars with size 2 bar (=6.35mm) double hoops spaced at 5” (=127mm). A double bending testing technique was used and specimens R-1 and R-5 had a total height of 96” (2438mm) and 72” (1829mm), respectively. Different longitudinal reinforcement steel grades (grade 40 for R-1 and grade 60 for R-5) were used. Axial loading was held constant at 507kN (σ_N=2.1MPa, equal to 5% of the axial load section capacity). The test results show a bending behaviour for the R-1 specimen with a small loss in peak strength. The shorter R-5 specimen clearly displayed brittle shear failure. The main features of the two specimens are summarised in Table 1. The assumed concrete properties are summarised in Table 2.

Each columns was modelled as a single bending element, with a shear span equal to the half member length. Integration over the element length is performed at two Gauss sections only so as to properly

assign to each section a tributary length that correspond to the actual length where damage take place in the physical model (a length slightly smaller than the section width). Longitudinal steel fibres are positioned where each individual longitudinal reinforcing bar was actually placed in the tested specimen. The equivalent transverse reinforcement ratio is calculated based on stirrup area and spacing.

Table 1: UC San Diego columns: main specimen features.

	R-1	*R-5*
steel ratio (%)	*2.5*	*2.5*
aspect ratio (-)	*2*	*1.5*
compression (MPa)	*-2.1*	*-2.1*
f_{cc} *(MPa)*	*-37.9*	*-32.7*
$f_{y,bars}$ *(MPa)*	*317*	*469*
$f_{y,hoops}$ *(MPa)*	*360*	*324*

Table 2: UC San Diego columns: additional concrete parameters used in the numerical simulations.

	R-1	*R-5*
ε_{cc} *(%)*	*0.25*	*0.22*
f_{ct} *(MPa)*	*3.5*	*3.0*
E_c *(GPa)*	*25*	*22*
v	*0.18*	*0.18*

Figure 7 (left) shows a good match between the force displacement curves found with the model and the experimental test of the R-1 specimen. The computed peak shear force (545kN for cyclic and 555kN for monotonic loading, respectively, corresponding to a maximum column displacement equal to 36mm) shows a good approximation with the test results (570kN). The numerical model does not trace the peak strength degradation. This is typical of fibre model's flexural response where the plain section assumption and perfect bond do not allow a full prediction of the response degradation.

The numerical analysis of specimen R-5 displays a brittle response, very clearly shown in figure 7 (right) for monotonic loading. It can be noted that for displacements larger than the value corresponding to the specimen peak strength (approximately 12mm), the numerical model response has a sudden strength drop that appears al larger displacements in the experimental test. The model maximum shear is somewhat lower than its experimental counterpart (700kN vs 742kN), whereas the column residual strength is well identified. Good results are also obtained for cyclic simulations (same figure 7 right). The model response shows both strength and stiffness degradations during the reloading phase when reaching the maximum negative imposed displacement (-12mm). During the second displacement cycle (17mm), the residual strength level is achieved by the confinement action of the hoops on the concrete fibres. Experimental data shows that specimen failure occurs during the first attempt at a maximum displacement amplitude equal to 17mm (precisely at a displacement value of 14.5mm). Such small discrepancies are well within acceptable limits.

The base section curvature and shear deformation are shown in figure 8 for monotonic loading. It is clearly shown that the model is able to trace the shear failure: at approximately 15mm top displacement, the section curvature ceases to increase following the attainment of the peak shear strength, and gradually drops at higher displacements before reaching an asymptote that basically indicates that the displacement increments are all due to the shear deformation that, on the other hand, increases rapidly beyond the 15 mm displacement level. This response follows the opening of a shear crack that yields large deformation rates at decreasing force levels.

Lastly, for monotonic loading, figure 9 shows the evolution of both section tangential stress and strain distributions. Specifically, the ε_{xy} distribution is highlighted. The dual section approach of the presented beam shear model shows that all the fibre deformation demand is on the tension side of the section. The presence of steel reinforcement, where axial tensile forces are exchanged between sections in the investigated equilibrium condition, generates the shear strain distribution correction coefficients. In accordance with the real physical phenomena, it is also found that the fibres in the compression zone are those responsible for the shear resistance of the section (the neutral axis is found at fibres 7-8).

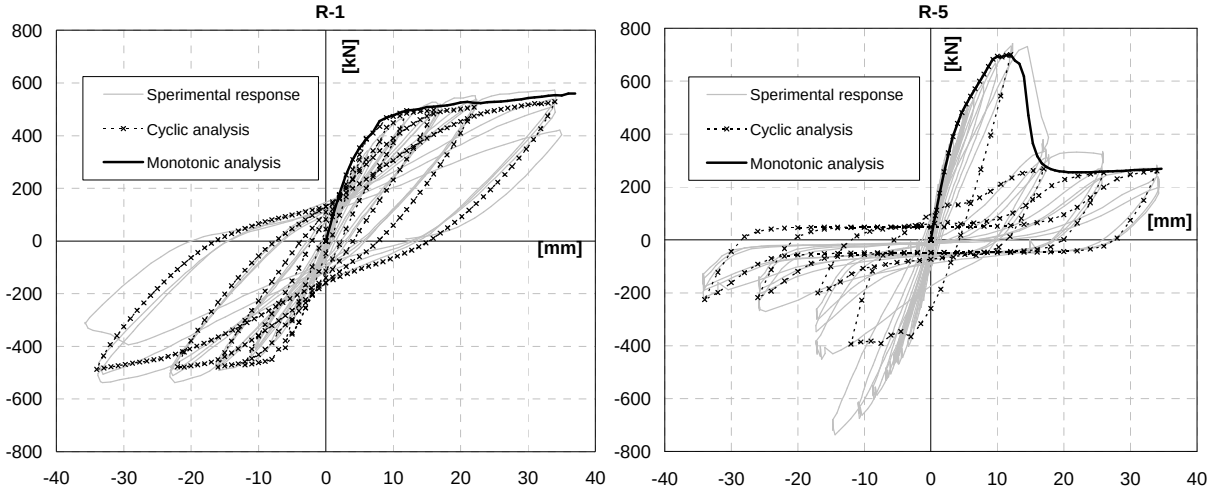

Figure 7: Base shear – top displacement specimens R-1 and R-5.

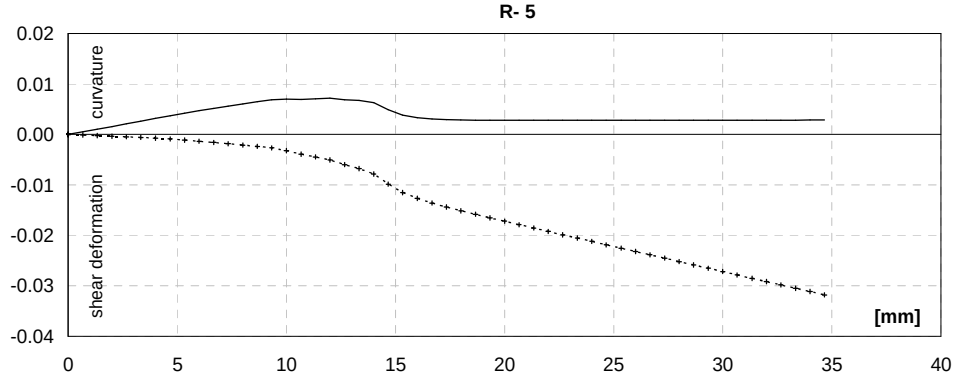

Figure 8: Specimen R-5, top displacement and section deformation (at 1st Gauss section) for monotonic analysis.

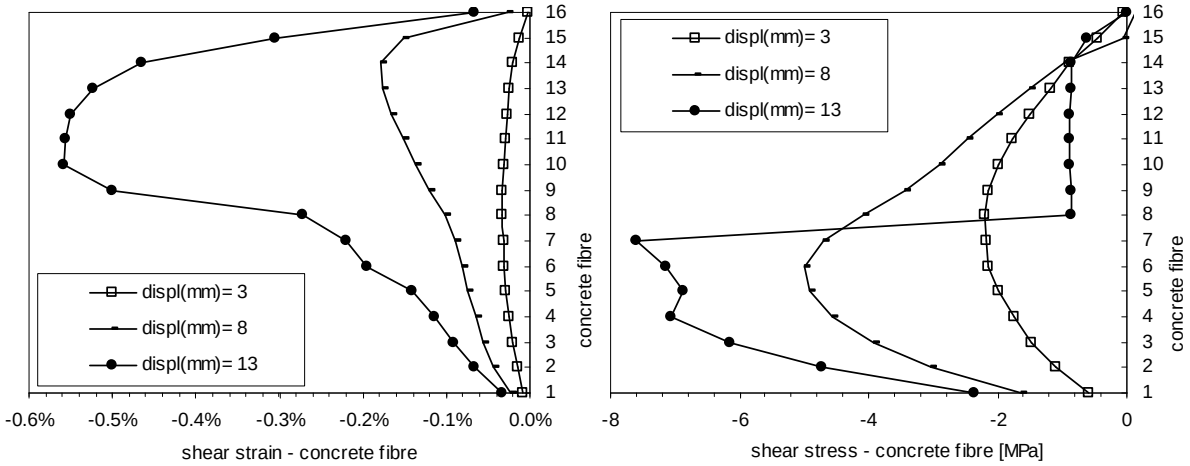

Figure 9: Specimen R-5, fibre shear stress and strain along the 1st section under monotonic analysis.

4. Conclusions

The paper describes the enhancement of a force-based fiber section beam element with shear deformations. The enhancement is mainly related to the introduction of the *Dual Section* procedure. It is shown that the new procedure successfully identifies shear failure mechanisms for reinforced concrete beam-column elements. The proposed model shows a good capability to corretl1y simulate

and predict the response of RC members under monotonic and cyclic conditions. The proposed model is particularly suited for the static and dynamic analysis of existing reinforced concrete frame structures.

It is noteworthy that the presented fibre beam model's effectiveness is to be ascribed to the use of a solid and efficient material constitutive law (microplane model) allowing realistic concrete response to be determined under different loading conditions.

References

[1] A Fibre/Timoshenko Beam Element in CASTEM2000, Guedes, J., Pegon, P., Pinto, A. V., Special Publication Nr. I.94.31 Applied Mechanics Unit, Safety Technology Institute, Commission of the European Communities, Joint Research Centre, Ispra Establishment, Italy, 1994.

[2] A numerical model for shear dominated bridge piers, Guedes, J., Pinto, A., Proc. of the second Italian-Japan Workshop on seismic design and retrofit of bridges, Roma, 1997.

[3] A fibre finite beam element with section shear modeling for seismic analysis of RC structures Ranzo, G., Petrangeli, M., J. of Earthquake Engineering, **2**(3), 443-473, 1998.

[4] Fibre element for cyclic bending and shear of RC structures. I: Theory, Petrangeli, M., Pinto, P.E., Ciampi, V., J. of Engineering Mechanics, ASCE, **125**(9), 994-1001, 1999.

[5] Fibre element for cyclic bending and shear of RC structures. II: Verification, Petrangeli, M., J of Engineering Mechanics, ASCE, **125**(9), 1002-1009, 1999.

[6] Predicting the response of reinforced concrete beams subjected to shear using Modified Compression Field Theory, Vecchio, F.J., Collins, M.P., ACI Structural Journal, **85**, 258-268, 1988.

[7] 3D frame element for the analysis of reinforced and prestressed concrete structures subjected to shear and torsion loads, Gregori J.N., Sosa P.M., Prada M.A.F., Filippou F.C., Engineering Structures, **29**(12), 3404-3419, 2007.

[8] A fibre flexure-shear model for seismic analysis of RC-framed structures, Ceresa P., Petrini L., Pinho R., R. Sousa.,. Earthquake Engineering and Structural Dynamics, **38**(5), 537-586, 2009.

[9] Mixed formulation of nonlinear beam finite element, Spacone, E., Ciampi, V., Filippou, F.C., Computers & Structures, **58**(1), 71-83, 1996.

[10] Equilibrium based iterative solutions for the nonlinear beam problem, Petrangeli M., Ciampi V., International J. of Numerical Methods in Engineering, **40**, 423-437, 1997.

[11] Method of analysis for cyclically loaded reinforced concrete plane frames including changes in geometry and non-elastic behavior of elements under combined normal force and bending, Menegotto, M., Pinto E., Proc. IABSE Symposium. Lisbon, Portugal, 1973.

[12] Un modello microplane modificato per la risposta del calcestruzzo nel piano, Tortolini, P., Petrangeli, M., Spacone, E.,. Atti XIII Congresso ANIDIS, Bologna, 28 giugno - 2 Luglio, 2009 (*in italian*).

[13] Microplane model for brittle plastic material. I: Theory, Bažant, Z.P., Prat, P.C., J. of Engineering Mechanics, ASCE, **114**(10), 1672-1688, 1988.

[14] L'elemento di trave non lineare con interazione M-N-V, Tortolini, P., PhD Dissertation, Univ. "G. D'Annunzio" of Chieti-Pescara, Italy, 2011 (*in Italian*).

[15] Theoretical stress-strain model for confined concrete, Mander, J.B., Priestley, M.J.N., Park, R., Journal of Engineering Mechanics, ASCE, **114**(8), 1804-1826, 1988.

[16] Steel jacket retrofit for enhancing shear strength of short rectangular reinforced concrete columns, Xiao Y., Report No. SSRP-92/07, University of California, San Diego, 1993.